LA-UR

LA-UR--90-4023

DE91 004861

. . . prepared by . . . under contract W-7405-ENG-36

TITLE EFFECT OF INTERNAL GAS PRESSURE ON THE SHOCK CONSOLIDATION OF 304 STAINLESS STEEL POWDERS

AUTHOR(S) Norman Eugene Elliott, MST-7
Karl Paul Staudhammer, MST-5

SUBMITTED TO International Conference on High Strain-Rate Phenomena in Materials
to be published by Marcel Dekker, New York, NY
August 13-16, 1990

DISCLAIMER

MASTER

Los Alamos National Laboratory
Los Alamos, New Mexico 87545

EFFECT OF INTERNAL GAS PRESSURE ON THE SHOCK CONSOLIDATION OF 304 STAINLESS STEEL POWDERS

N. E. ELLIOTT and K. P. STAUDHAMMER

Los Alamos National Laboratory
Materials Science and Technology Division
Los Alamos, New Mexico 87545 U.S.A.

Capsules of 316 SS powders having a pre-compacted density of 67% were shock consolidated at peak pressures of 130 GPa. Initial internal Ar gas pressures from 3×10⁻⁴ Pa to 1.1 MPa were employed. However, as the internal Ar gas pressure in the powders was increased, the quality of the compacted density decreased. While it is intuitive that high internal gas pressures in porous materials do not enhance their consolidation, a greater understanding of the consolidation process and the part entrapped intentional or unintentional gas plays is elucidated.

1. INTRODUCTION

When powder in a container is consolidated, the initial bulk density dictates the volume change that is required to produce a solid compact. The arrangement of the particles and the consequent distribution of voids between the particles has a major influence on the subsequent behavior of the powder mass. In the consolidation process powder must

undergo rapid deformation and flow to eliminate the void space and form strong interparticle bonds. This process of densification and interparticle bonding is very complex and is strongly dependent on any residual (intentional or unintentional) gas in the void pockets. Gas presence in a pre-compacted sample can have a significant effect on the quality of the resulting compacted monoliths. In fact, earlier attempts [1] to shock consolidate metal powders using optimum shock pressures under atmospheric gas pressures in the pre-compacted powder resulted in poor consolidation and/or fractional melting of the powders. Initial solutions to this employed vacuum outgassing of consolidated monoliths [5], and to evacuate the initial compact prior to shock consolidation. To a large extent both methods appeared to work. However, vacuum outgassing after consolidation did not prove to be convenient or practical. On the other hand, pre-evacuating, did produce better results and was thought to be the best obtainable. The vacuum that many investigators were achieving, however, was not a "hard" vacuum, but rather just a reduced internal pressure. The residual pressure resulting from gas trapped in the pores of the metal powders produced variations in the results and interpretation of vacuum prepared specimens. In fact, pre-evacuation of capsules containing samples of metal powders in the size range of 50 to 250 mm at approximately 65% packing density act as "virtual leaks" to a pumping system [7,8]. It is extremely difficult to remove the entrapped gases by pumping on them, even to the extent of a few days. To truly obtain very low internal pressures ($<10^{-3}$ Pa) other methods such as moderate temperature bake out under vacuum must be employed.

The effect of residual internal gas pressure on the shock consolidation process can be demonstrated by the use of fig.1. In fig.1 the Hugoniot compressibility of a porous material is shown generically. This Hugoniot curve is for a porous system having an "ideal vacuum" environment in the pores. Any residual gas environment even at 10^{-1} Pa would shift the release isotrope towards the right (lower compaction) due to the compressibility of the entrapped gas that cannot leave the system. Thus the Hugoniot as shown in fig.1 is only an approximate representation as one approaches very low residual gas pressures. Practically, as we will show with the experiments performed here, residual pressure as low as 10^{-1} Pa has a profound effect on the consolidated monolith, preventing full consolidation. In fact, an understanding of internal gas pressure and its accumulative effect on the consolidation process is essential in the production of optimum monoliths. However, such an understanding is not only applicable to the consolidation process but also among other things, to shock synthesis.

II. EXPERIMENTAL

Samples of Valimet 304SS -70/320 mesh powder were exposed to similar shock conditions. The pre-shock internal gas pressure varied over the range of best obtainable vacuum to roughly 0.1GPa of N_2 gas. The conditions are summarized in the following table:

Pressure N_2 gas (Pa)	Molar ratio N_2/304SS	Starting density	range of shock pressure
$7x10^{-4}$	10^{-12}	~67% theoretical	10^8 Pa
10^5	10^{-4}	~67% theoretical	to
10^7	10^{-2}	~67% theoretical	$4x10^8$ Pa
10^8	10^{-1}	~67% theoretical	

The internal gas environments of the samples were produced as follows:

* $7x10^{-4}$ Pa- The 304SS powder was placed in a 304SS tube and evacuated to roughly 10^{-3} Pa. The system was then backfilled to atmosphere with dry nitrogen gas. This process was repeated 3 times. The sample was then left on the vacuum system for 4 days with periodic external vibration to increase pumping speed in the fine pores of the powder. At this point the sample was valved off from the pumping system and the pressure rise with time noted. After four days of pumping, "virtual leaks" from the porous powder were still being observed. The pressure recorded was not the lowest obtained but an estimate of the equilibrium resulting from the trapped gas. A pinch weld in a brazed copper end piece was made to preserve the vacuum. The sample was explosively compacted roughly one hour after being removed from the pumping system.
* 10^5 Pa- Were prepared similarly to the vacuum sample by backfilling with dry nitrogen from roughly 10^{-3} Pa and pinch welded.
* 10^7 and 10^8 Pa- The samples were placed in commercial 316 stainless steel high pressure tubing and pressurized with dry N_2. Commercial high pressure valves were used to maintain internal pressure until explosive compaction. The design of the assembly allowed the passing shock wave to pinch off the tubing after passage through the sample, separating the valve assembly and leaving the sample for post shock analysis and is shown schematically in fig.2.

Various versions of the shock design have been described previously [8-10]. Post shock analysis was carried out by a variety of techniques. The primary method of analysis was Scanning Electron Microscopy (SEM) supported by optical microscopy. Energy Dispersive Analysis (EDX) was used to confirm chemical analysis. X-ray diffraction (XRD) was used to determine texturing of the powders produced by the shock event. The post shocked samples were cut perpendicular to the central axis at selected distances correlating to specific

shock pressures. Metallographic samples were chemically etched by standard techniques prior to analysis.

III. RESULTS AND DISCUSSION

Shown in fig.3 are the overview cross section at equivalent shock pressures of 0.4 GPA for the range of internal gas pressures form $7x10^{-4}$ Pa (fig.4a) to 10^8 Pa (fig.3d). The best consolidation was achieved with the "best vacuum" condition of $7x10^{-4}$ Pa. At 10^5 Pa and 10^7 Pa (fig.3b,c) the resultant structure shows less consolidation, however, reasonably well compacted regions exist within each sample. At 10^8 Pa the structure is very loosely compacted with minimal particle bonding. In fact many of the powder particles were lost, some due to metallographic preparation, but in general most were lost as a result of shock venting of the sample holder. It should be noted that the sample holder for the 10^8 Pa, N_2 pressure (fig.3d) had a smaller internal diameter than those shown in figs.3a-c. This was necessary to accommodate the high internal gas pressure. In comparison to the shock pressure, an internal pressure of 10^8 Pa has a significant cooling effect upon release just after shock wave passage. Thus, the lack of melting at the inner core nearest the Mach stem that was present in fig.3b with an initial pressure of 10^5 Pa. In addition, the vented gas exits with a far greater velocity at the higher pressure and has the capability to carry with it those particles which are not sufficiently anchored in the matrix. Samples consolidated at a lower shock pressure of 0.1 GPa are shown in fig.4. The quality of consolidation is evident for these series of micrographs, as well as, the degree of porosity. Clearly, the effect of internal N_2 gas pressure is particularly evident in 4c and d, where consolidation was not achieved. A more detailed SEM microstructure is shown in fig.5 taken from fig.4d. The regions marked A are backfilled epoxy material used for the metallographic preparation of the samples. The structure of the particles show little deformation and no melting of the particle surfaces or near interstices of the pore collapse as was evident in portions of fig.4a. The obvious lack of melting particularly at the pore sites is shown in fig.5c-d. Even at the higher pressure (fig.5d) melting is not observed. Figure 6 is a schematic representation of the increase in temperature resulting from the shock event. There are actually three major contributions, the adiabatic, residual and stram which are discussed in an earlier paper [12]. The combined effect of these factors is shown as the line labelled "Solid". However, for a porous sample, the temperature rise is much greater due to the collapse in volume and the resulting large stram temperature contribution as depicted in fig.6. Additionally, the temperature increases with shock compression of an enclosed or entrapped gas in the pores. The entrapped gas has different compressibility than the matrix metal powder and upon passage of the shock wave the gas remains behind in a smaller volume, at greater pressure and at a higher energy state.

This results in a net increase in the overall temperature. The internal gas pressure decreases the "quality" of consolidation via excess temperature resulting in localized melting and/or cracking of the consolidated compact. At very high internal gas pressures, the gas can have a very detrimental effect and prevent particle to particle bonding even though the adiabatic temperature may exceed melting. This results from the high internal gas pressure preventing particle contact.

An attempt to explain the increase in temperature resulting from shock compression of the higher internal gas pressure can be illustrated in fig.7. Temperature profiles as a function of time, for shocked samples involves a complex combination of events. The initial adiabatic compression causes the temperature of all samples to rise along a similar path. However, after passage of the shock wave the amount of residual strain, non-adiabatic gas heating and heat of reaction cause the sample to cool along different paths as indicated in fig.3. The time scale for these events is much longer than that of the shock wave itself and the specimen temperature is lowered. None the less, it is in this regime where many of the observed events of chemical and metallurgical significance occur.

The relationship of strain and non-adiabatic heating is illustrative of this point. In the case of a hard vacuum, a monolith with essentially no porosity can be obtained. The post shock temperature is a result of heating caused by the deformation of individual particles to fill the interparticle voids. As the pressure of internal trapped gas in collapsing voids increases, the situation changes. At lower starting internal pressures, the individual particles still deform although not to complete void collapse. As the pressure in the collapsing void reaches the shock pressure the internal gas becomes trapped. This results in heating from a combination of local strain in the particles filling collapsing voids, and non-adiabatic heating resulting from compressed gas trapped in the porous monolith. At the extreme where the starting internal pressure is a significant fraction of the shock pressure, little strain is observed. Individual particles are essentially undeformed fig.4d,5d. Internal gas pressure vented immediately after passage of the shock wave since no closed pockets have formed. The rapid drop in pressure results in modest cooling of the sample below the starting conditions. This effect was observed empirically during tests. Initially all samples could be handled immediately after explosive compaction. As time passed, the high strain, low internal pressure samples warmed as heat from the interior reached the surface. In the case of low stain, high internal pressure, the samples never became hot. The amount of this strain was measured more directly by x-ray diffraction as shown in fig.8. The ratio of the intensity of the (220)/(200) reflections are indicative of internal particle strain and are plotted in fig.9. The overall strain in all samples was about 3% as measured by the elongation of the sample holders. This amount would normally not be detected by x-ray diffraction. The amount of deformation in individual particles is much greater due to void collapse and can be detected. The sample with the highest internal

pressure showed essentially no difference from the original starting powder. The sample with the lowest internal pressure exhibited significant preferential texturing as a result of deformation as measured by XRD. The type of texturing produced in the samples with low internal pressure, high strain is similar to that observed for mechanically drawn material. This is consistent with the cylindrical geometry of the shock assembly.

IV. CONCLUSIONS

Consolidation is directly proportional to the initial internal gas environment of powder specimens. We have observed measurable effects with starting gas pressure less than atmospheric. Because of the difficulty in obtaining vacuum in powder specimens care must be exercised in interpreting results from experiments conducted under nominal but uncertain vacuum conditions. The use of *controlled* gas environments can significantly enhance a variety of shock consolidation processes. in particular, shock synthesis can successfully employ these results.

REFERENCES

1. *Fifth International Conference on High Energy Rate Fabrication*. Chap. 5. Denver, CO.June 1975

2. D. Raybould, *J. Mat. Sci., 16:* 589 (1981)

3. W. H. Gourdin, *J. Appl. Phys., 55:* 172 (1984)

4. D. Morris, *J. Matl. Sci., 17:* 1789 (1982)

5. R. Prümmer, *Vortrag 4:* 10 (1972)

6. John F. O'Hanlon, *A User's Guide to Vacuum Technology*, John Wiley and Sons, New York, NY. Chap.2/3, 1980

7. A. Roth, *Vacuum Technology*, North Holland Pub., Amsterdam, Holland Chap.4, 1979

8. K. P. Staudhammer and L. E. Murr, *J. of Matl. Sci. 25:* 2287 (1990)

9. K. P. Staudhammer and L. E. Murr, *Shock Waves for Industrial Applications*, L. E. Murr ed., Noyes Pub., New York, 1988 p.237.

10. K. P. Staudhammer and K. A. Johnson,*Metallurgical Applications of Shock Wave and High Strain Rate Phenomena*,L. E. Murr, K. P. Staudhammer and M. A. Meyers eds., Chap.7, Marcel Dekker, New York, 1986 p. 149.

11. K. P. Staudhammer and K. A. Johnson, *Proceedings of the International Symposium on the Intense Dynamic Loading and Its Effects*, Z. Zhemin and D. Jing eds., Science Press, Beijing China, 1986

12. K. P Staudhammer, *Shock Compression of Condensed Matter - 1989*, S. C. Schmidt, J. N. Johnson and L. W. Davidson eds, Elsevier Science Pub. B.V., 1990 p. 519.

ACKNOWLEDGEMENTS

We wish to thank A. Bonner and R. Medina for their helpful support and logistics at the firing site, and to A. J. Gray for the mettallographic preparation. This work was supported by the DOE under contract W-7405-ENG-36.

FIGURE CAPTIONS

FIG. 1 *Schematic of shock pressure versus volume Hugoniot.*

FIG. 2 *Schematic of high internal gas pressure shock system.*

FIG. 3 *Optical micrographs of 0.4 GPa shocked samples as a function of a) 7×10^{-4} Pa, b) 10^5 Pa, c) 10^7 Pa, and d) 10^8 Pa internal N_2 gas pressure.*

FIG. 4 *Optical micrographs of 0.1 GPa shocked samples as a function of a) 7×10^{-4} Pa, b) 10^5 Pa, c) 10^7 Pa, and d) 10^8 Pa internal N_2 gas pressure.*

FIG. 5 *SEM backscatter electron images of shocked 10^8 Pa internal N_2 gas pressure as a function of a,c) 0.1 GPa shock pressure and b,d) 0.2 GPa shock pressure.*

FIG. 6 *Schematic representation of temperature increase with pressure for solid and porous materials. For porous materials the final temperature is strongly dependent on the closed porosity.*

FIG. 7 *Schematic of temperature versus time as a function of internal gas pressure. Illustrating a maximum temperature effect as a function of increasing internal gas pressure.*

FIG. 8 *X-ray diffraction pattern of the starting powder and shocked (0.4 GPa) samples containing the indicated internal gas pressure.*

FIG. 9 *Ratio of the (220) (200) peaks as a function of the internal gas pressure from the data shown in Fig.8. The ratio is indicative of the amount of retained γ in the powder.*

FIGURE CAPTIONS

FIG. 1 Schematic of shock pressure versus volume Hugoniot.

FIG. 2 Schematic of high internal gas pressure shock system.

FIG. 3 Optical micrographs of [illegible].4 GPa shocked samples as a function of a) 7 X 10^{-4} Pa, b) 10^5 Pa, c) 10^7 Pa, and d) 10^8 Pa internal N_2 gas pressure.

FIG. 4 Optical micrographs of [illegible].1 GPa shocked samples as a function of a) 7 X 10^{-4} Pa, b) 10^5 Pa, c) 10^7 Pa, and d) 10^8 Pa internal N_2 gas pressure.

FIG. 5 SEM backscatter electron images of shocked 10^8 Pa internal N_2 gas pressure as a function of a,c) [illegible].1 GPa shock pressure and b,d) [illegible] GPa shock pressure.

FIG. 6 Schematic representation of temperature increase with pressure for solid and porous materials. For porous materials the final temperature is strongly dependent on the [illegible] porosity.

FIG. 7 Schematic of temperature [illegible] time as a function of internal gas pressure. [illegible] maximum [illegible] as a function of increasing internal gas pressure.

FIG. 8 X-ray diffraction pattern of the starting powder and packed bed of the samples containing the indicated internal gas pressure.

FIG. 9 Ratio of the (220) (200) peaks as a function of the internal gas pressure from the data shown in FIG. 8. The ratio is indicative of the amount of strain in the powder.

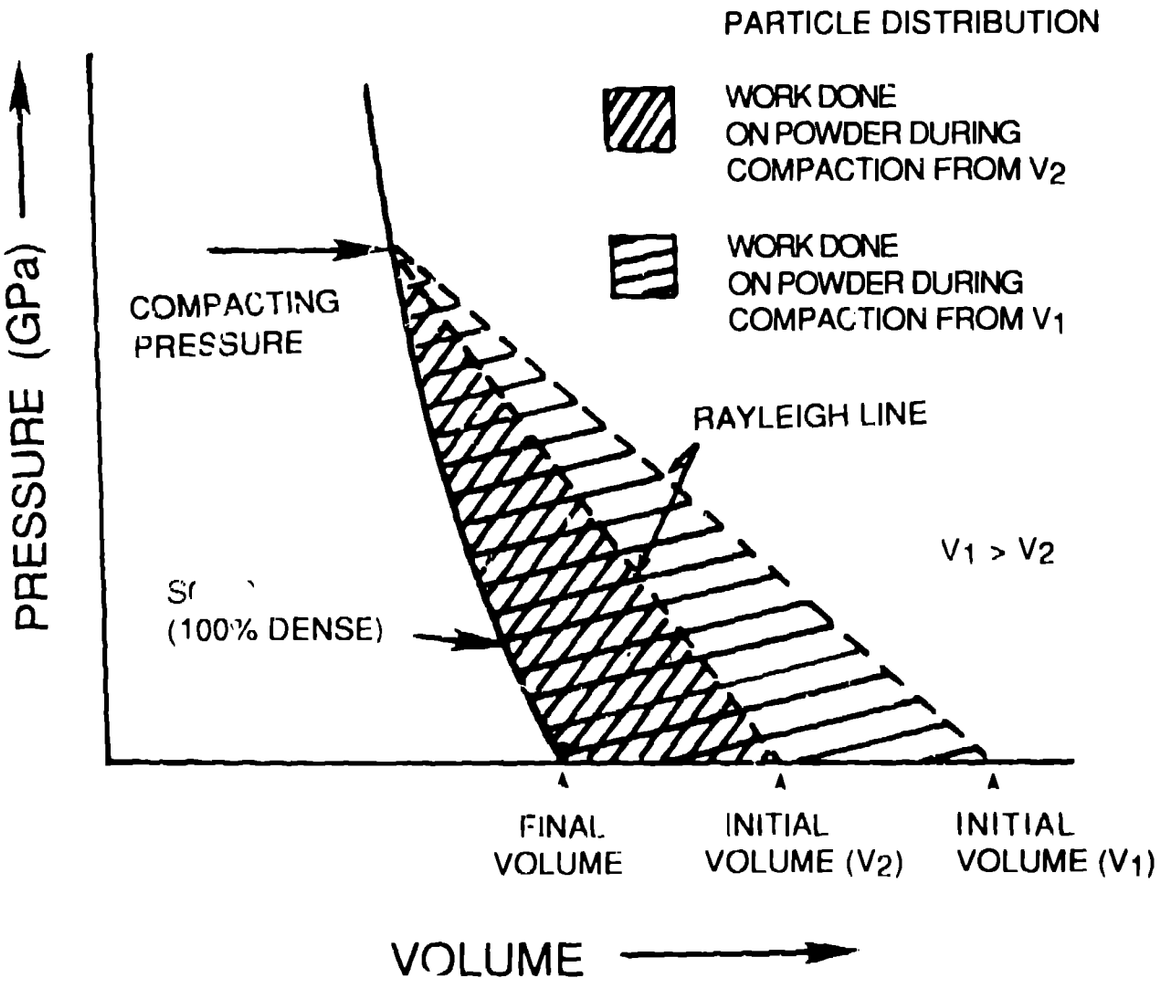
PARTICLE DISTRIBUTION
WORK DONE ON POWDER DURING COMPACTION FROM V_2
WORK DONE ON POWDER DURING COMPACTION FROM V_1
COMPACTING PRESSURE
RAYLEIGH LINE
$V_1 > V_2$
(100% DENSE)
PRESSURE (GPa)
FINAL VOLUME
INITIAL VOLUME (V_2)
INITIAL VOLUME (V_1)
VOLUME

SCHEMATIC OF HIGH INTERNAL GAS PRESSURE SYSTEM

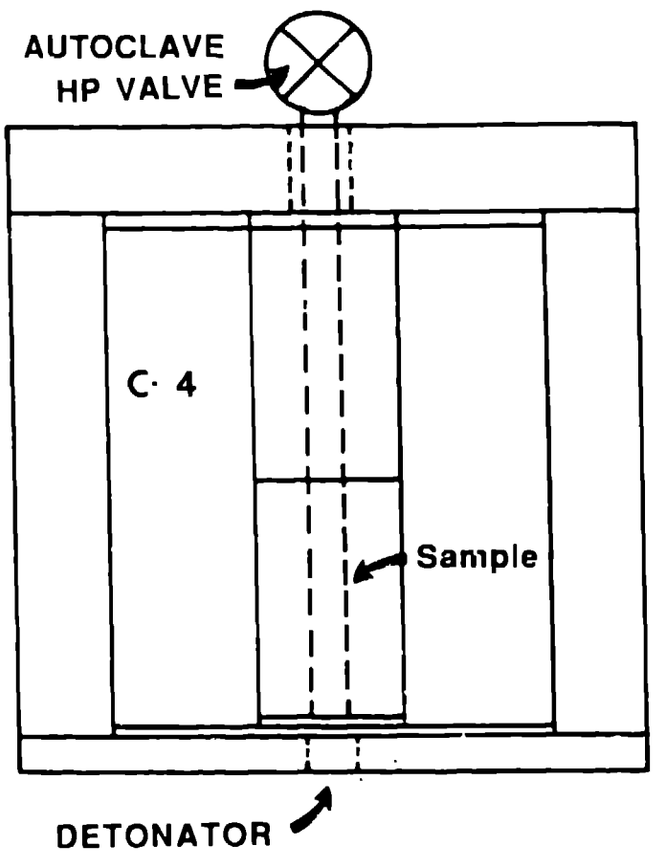

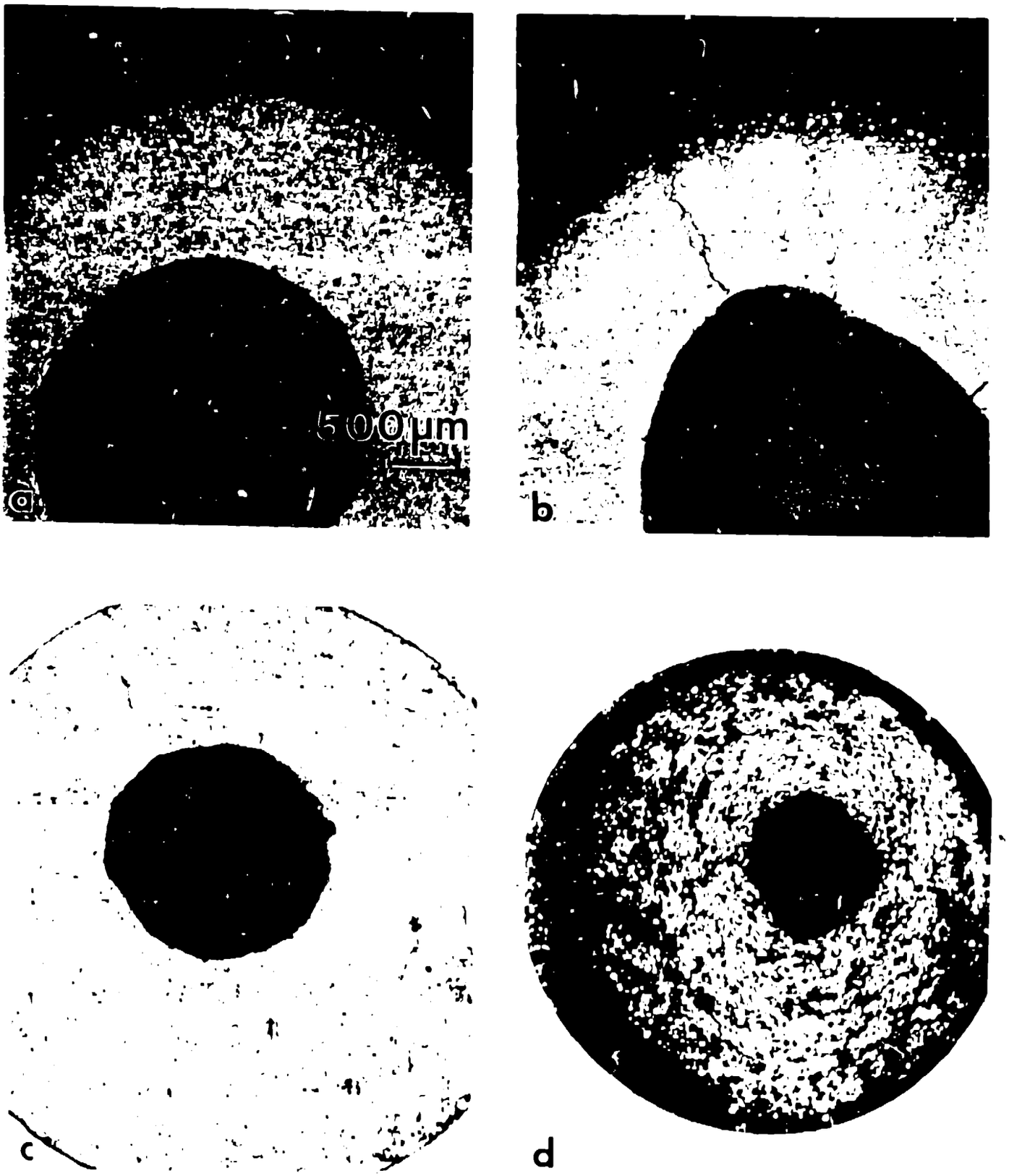
500µm
a
b
c
d

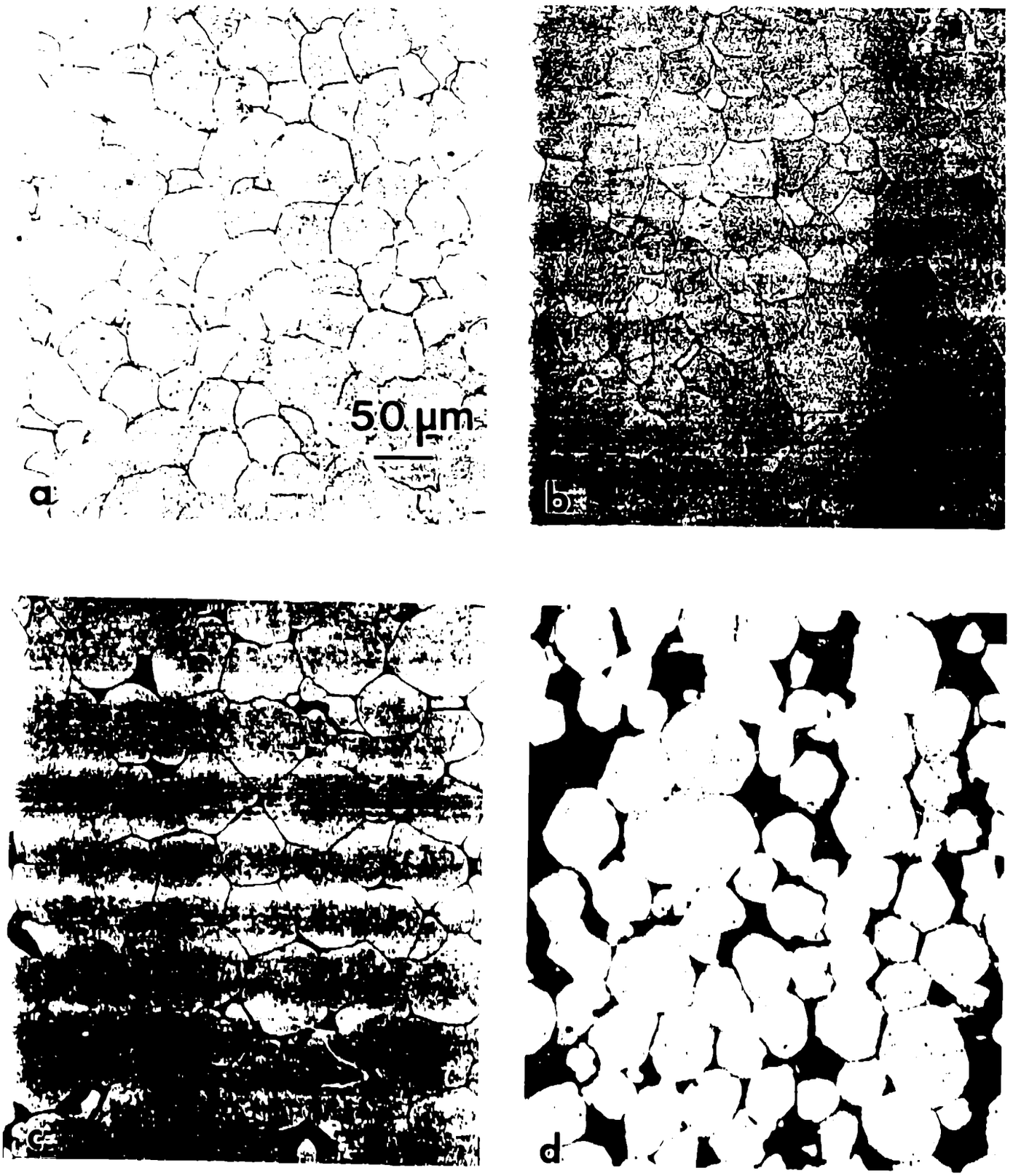
50 µm
a
b
c
d

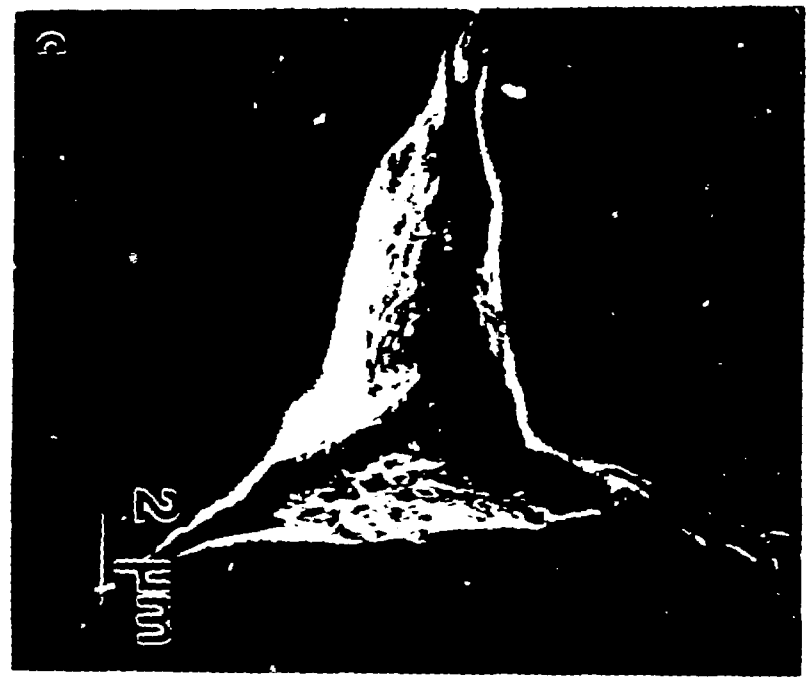
c)
2 μm

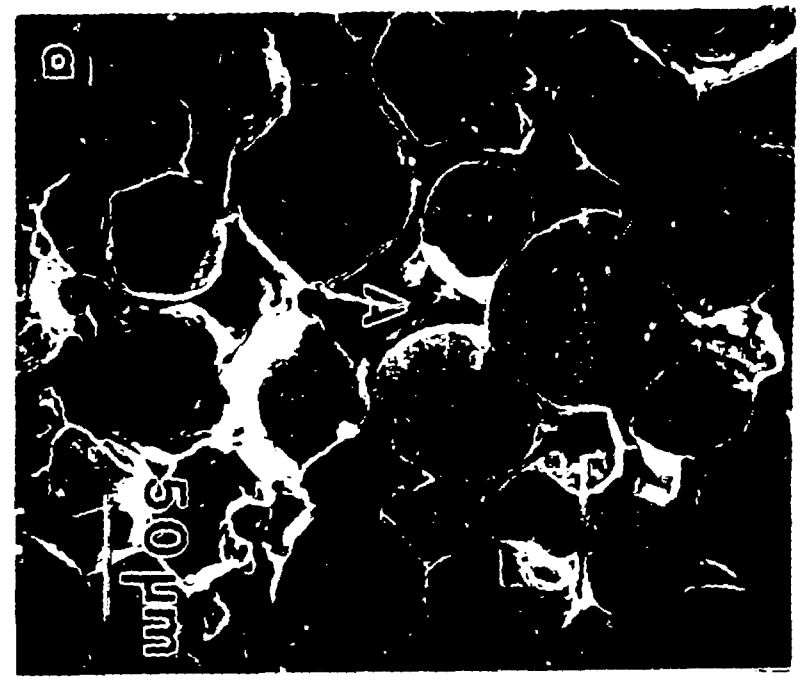
b)
50 μm


c)
2 μm

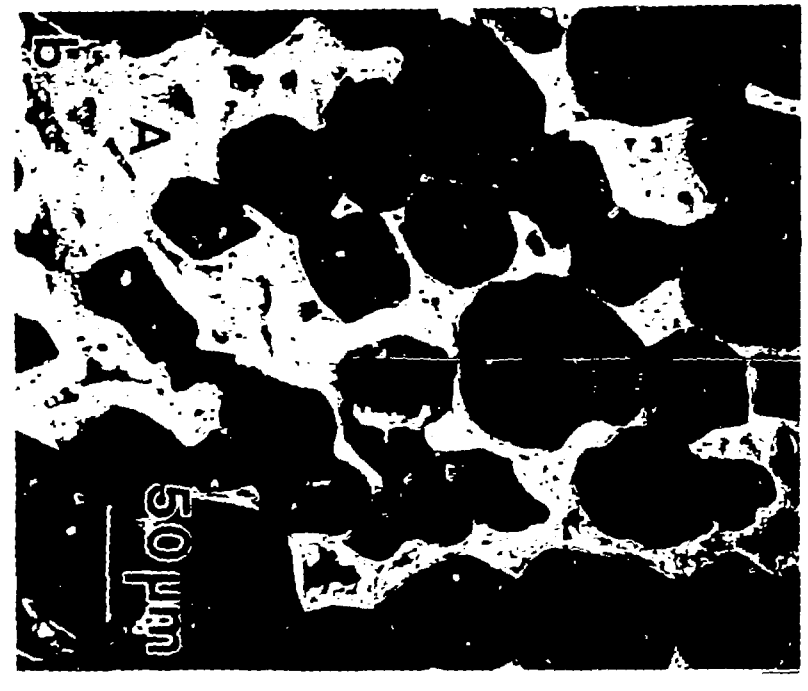
b)
50 μm

T vs P of Solid and Porous Samples

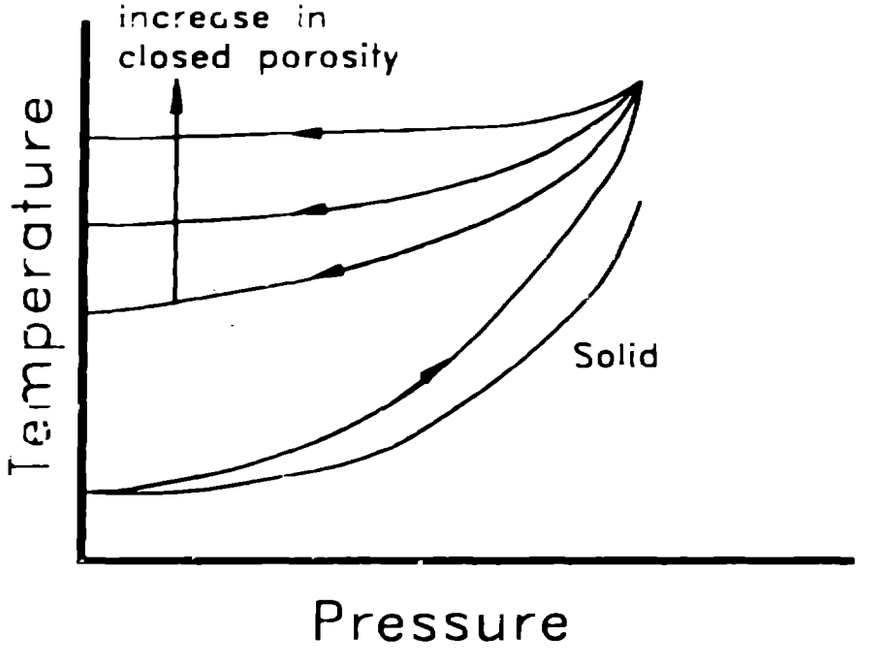

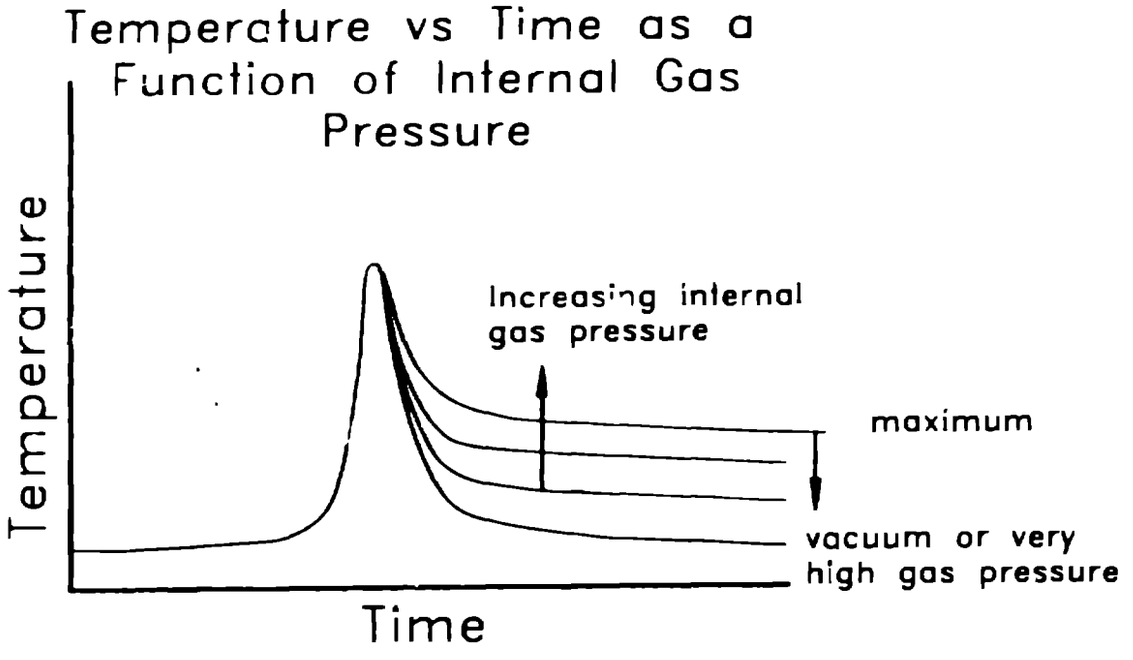
Temperature vs Time as a Function of Internal Gas Pressure
Temperature
Time
Increasing internal gas pressure
maximum
vacuum or very high gas pressure

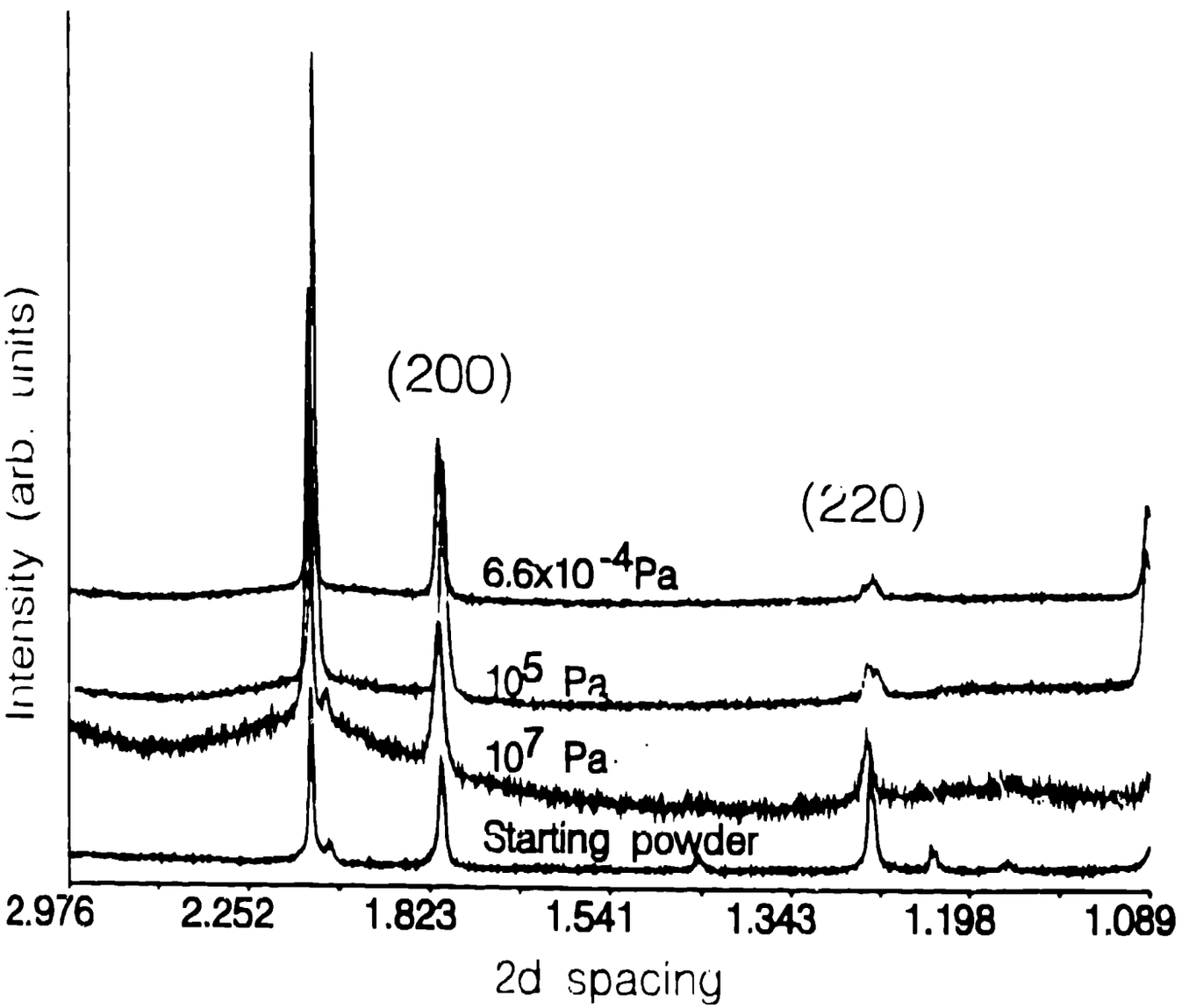
Intensity (arb. units)
(200)
(220)
6.6x10^{-4}Pa
10^5 Pa
10^7 Pa
Starting powder
2.976
2.252
1.823
1.541
1.343
1.198
1.089
2d spacing

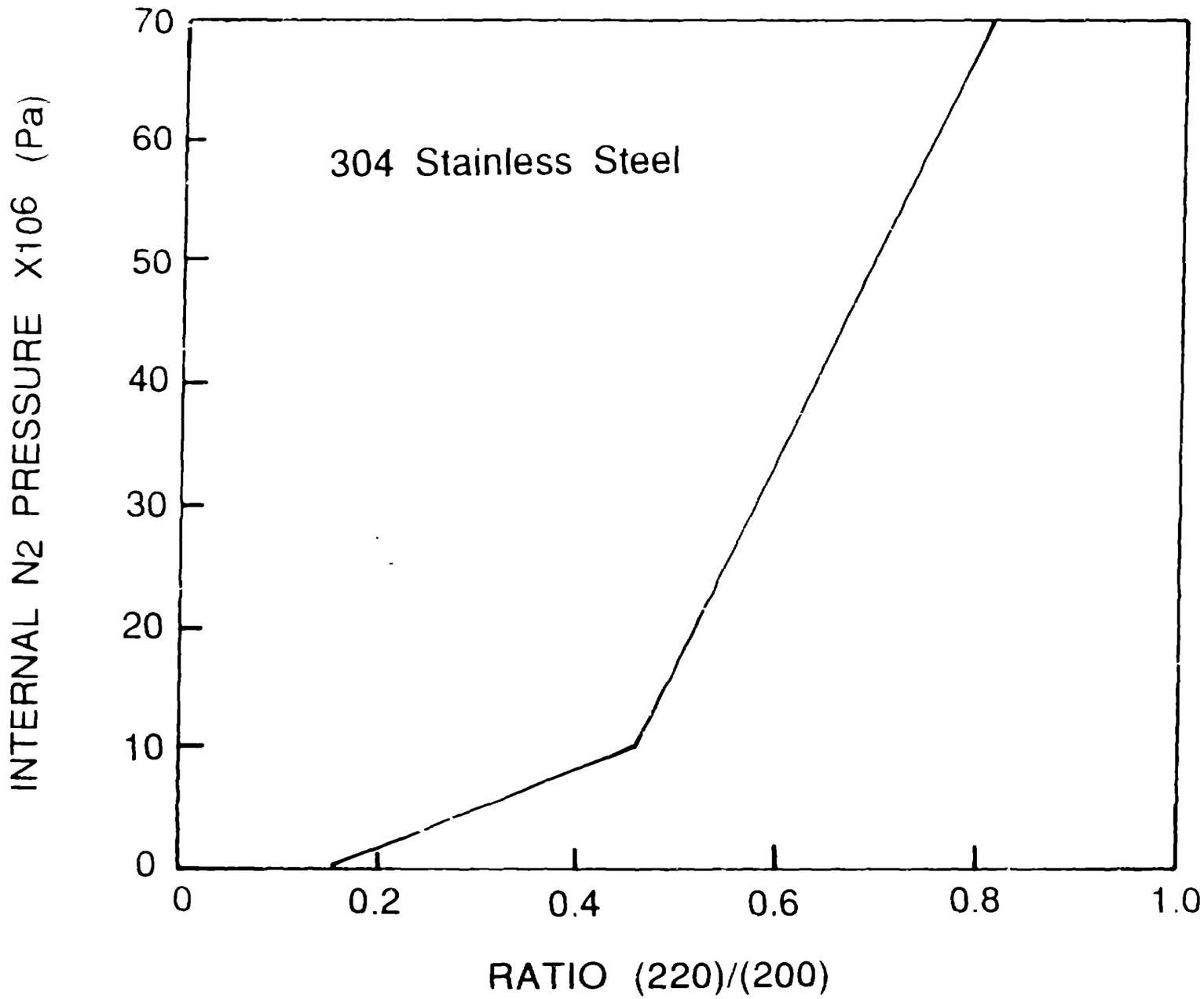
304 Stainless Steel
INTERNAL N2 PRESSURE X106 (Pa)
70
60
50
40
30
20
10
0
0
0.2
0.4
0.6
0.8
1.0
RATIO (220)/(200)